inorganics

MDPI

Article

Synthesis, Structural Characterization, Cytotoxicity, and Antibacterial Properties of Gold(III) Complexes with Hydrazones Derived from Vitamin B_6

Daria V. Petrova [1], Aleksandra K. Isagulieva [2], Olga N. Sineva [3], Vera S. Sadykova [3], Maksim N. Zavalishin [4] and George A. Gamov [4,*]

[1] The Institute for Physics of Microstructures, Russian Academy of Sciences, Nizhny Novgorod Region, Akademicheskaya St. 7, Afonino 603087, Russia; petrovadar@ipmras.ru
[2] Burnazyan Federal Medical Biophysical Center, Federal Medical Biological Agency, Marshal Novikov St., 23, Moscow 123098, Russia; kia2303@yandex.ru
[3] Gause Institute of New Antibiotics, Russian Academy of Sciences, Bol'shaya Pirogovskaya St. 11/1, Moscow 119021, Russia; olga.sineva81@yandex.ru (O.N.S.); sadykova_09@mail.ru (V.S.S.)
[4] General Chemical Technology Department, Ivanovo State University of Chemistry and Technology, Sheremetevskii Ave. 7, Ivanovo 153000, Russia; zavalishin00@gmail.com
* Correspondence: ggamov@isuct.ru; Tel.: +7-(915)-821-85-62

Abstract

The rise in the number of cancer cases and the dissemination of strains with multiple drug resistance in the world pose a serious threat to public health care and human well-being. The design and study of new chemotherapeutic agents for cancer and infectious diseases are hot topics in science. Hydrazones, a versatile and diverse class of chemical compounds, gained a lot of attention as a promising base for future drugs. In this paper, we report on the synthesis of eight new gold(III) complexes with hydrazones derived from pyridoxal-5′-phosphate and pyridoxal. The complexes are thoroughly characterized using IR, ^{1}H, ^{31}P NMR, and mass spectroscopy. The cytotoxic effect of twelve various hydrazones derived from pyridoxal 5′-phosphate on both immortalized (HEK293T) and tumor (HCT116) human cell lines was estimated using the MTT assay. In addition, this contribution describes the antibacterial action of complexes of gold(III) and pyridoxal and pyridoxal 5′-phosphate-derived hydrazones, as well as the mixtures of the solutions containing tetrachloroaurate(III) and hydrazones, using the zone of inhibition test. Gold(III) complexes exhibit moderate antibacterial activity against both Gram-positive and Gram-negative bacteria, while free hydrazones show low cytotoxicity and thus could be considered relatively safe for humans.

Keywords: hydrazone; gold(III); anti-tumor; antibacterial; complex; MTT; zone of growth inhibition

check for updates

Academic Editors: Dinorah Gambino and Esteban Rodríguez-Arce

Received: 23 September 2025
Revised: 8 October 2025
Accepted: 10 October 2025
Published: 11 October 2025

Citation: Petrova, D.V.; Isagulieva, A.K.; Sineva, O.N.; Sadykova, V.S.; Zavalishin, M.N.; Gamov, G.A. Synthesis, Structural Characterization, Cytotoxicity, and Antibacterial Properties of Gold(III) Complexes with Hydrazones Derived from Vitamin B_6. *Inorganics* **2025**, *13*, 335. https://doi.org/10.3390/inorganics13100335

Copyright: © 2025 by the authors. Licensee MDPI, Basel, Switzerland. This article is an open access article distributed under the terms and conditions of the Creative Commons Attribution (CC BY) license (https://creativecommons.org/licenses/by/4.0/).

1. Introduction

In recent years, the International Agency for Research on Cancer, working under the aegis of the World Health Organization, has indicated the growth of the global cancer burden and predicts a 77% increase from the estimated 20 million cases in 2022 to 2050 [1]. The dissemination of pathogens with multiple drug resistance poses no less threat [2]. The efforts of researchers all over the world are focused on developing new tools for combating bacterial infections and oncologic diseases. The design of new chemotherapeutics is a popular research area.

Schiff bases and hydrazones bearing the active pharmacophore groups (-N=CH- and -NH-N=CH-, respectively) are often used as a base for drug development because of the synthetic simplicity and ease of chemical modification [3,4]. Because of the latter, the fine-tuning of their cytotoxicity and beneficial action is achievable [5]. The representatives of both classes show various biological activities, including anti-oxidant, α-glucosidase and xanthine oxidase inhibition, anti-diabetic, anti-viral, anti-convulsant, and anti-inflammatory effects [6]. The anti-tumor properties of the different Schiff bases and hydrazones are also the subject of extensive research. Imines were tried as lead compounds for the treatment of breast [6–11], colon [8,12,13], prostate [14], nerve tissue [15], brain [9], lung [10,16], liver [10,17], and ovarian [11] cancer cells, as well as lymphoblast [8]. The paper [18] should be mentioned as it contains information about the cytotoxicity of the hydrazone derivative vs. a great deal of different cancer cell cultures. Complex formation with metal ions such as copper(II) [7] and tin(IV) [14] allows for making the hydrazones more cytotoxic.

The studies of the antibacterial activity of hydrazones are also numerous [19–23]. Among the hydrazones allowed for the clinical treatment of bacterial infections, nifuroxazide is arguably the most well-known example [24]. Lately, the repositioning of nifuroxazide for various types of cancer has been actively discussed [25]. Ftivazide, a hydrazone derived from vanillic aldehyde and isoniazid, is also a known anti-tubercular drug (although less active than starting hydrazide; the same applies to other isoniazid hydrazones [26]).

Metal complexes of hydrazones may also prove more efficient against bacteria than free ligands [19]. In general, the chelating ability of hydrazones and Schiff bases might be instrumental in combating pathogens as compounds deprive cells of essential metals [27]. In addition, it is noteworthy that hydrazones and Schiff bases are often used as efficient fluorescent sensors of metal ions [28–32], anions [33–35], and other molecules [36–38], which makes them suitable for bioimaging and theranostic purposes.

B_6 vitamin is one of the essential compounds in biochemistry as it serves as a coenzyme for numerous activities [39–41]. As a consequence, influencing its metabolism might be a promising way to fight against cancer [42–46].

Hydrazones and Schiff bases derived from aldehyde forms of the B_6 vitamin attracted a lot of attention for a long time [47], as they were found to be efficient iron chelators, which provided them with various beneficial properties, such as treating thalassemia, anti-oxidant, and anti-proliferative effects [47–56]. At the same time, some toxicity related to their metal-binding properties should also be noted [57,58]. Metal complexes of vitamin B_6-derived imines and hydrazones were a subject of thorough study (see, e.g., a review [59] or a recent review [60], which focuses on analytical uses of pyridoxal- and pyridoxal 5′-phosphate-derived Schiff bases and hydrazones for colorimetric and fluorimetric probing of various metal ions) as they can show anti-tumor effects [53]. Protolytic [61] and complexation [62] equilibria of such hydrazones were studied in aqueous solution. Gold(III), whose complexes are isoelectronic and isostructural to cisplatin, is often viewed as a suitable metal to synthesize coordination compounds with anti-tumor [63,64] and antibacterial [65] action. In this contribution, we synthesized several new gold(III) complexes derived from vitamin B_6 hydrazones and studied their antibacterial properties against Gram-positive and Gram-negative bacteria. In addition, we report on the cytotoxic effects of a series of vitamin B_6 hydrazones. The structural formulas of the compounds under study are given in Figure 1.

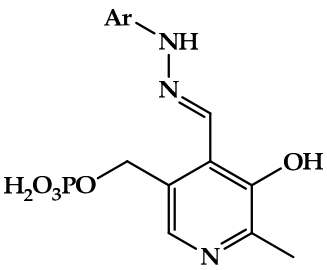

1a-l

Ar:

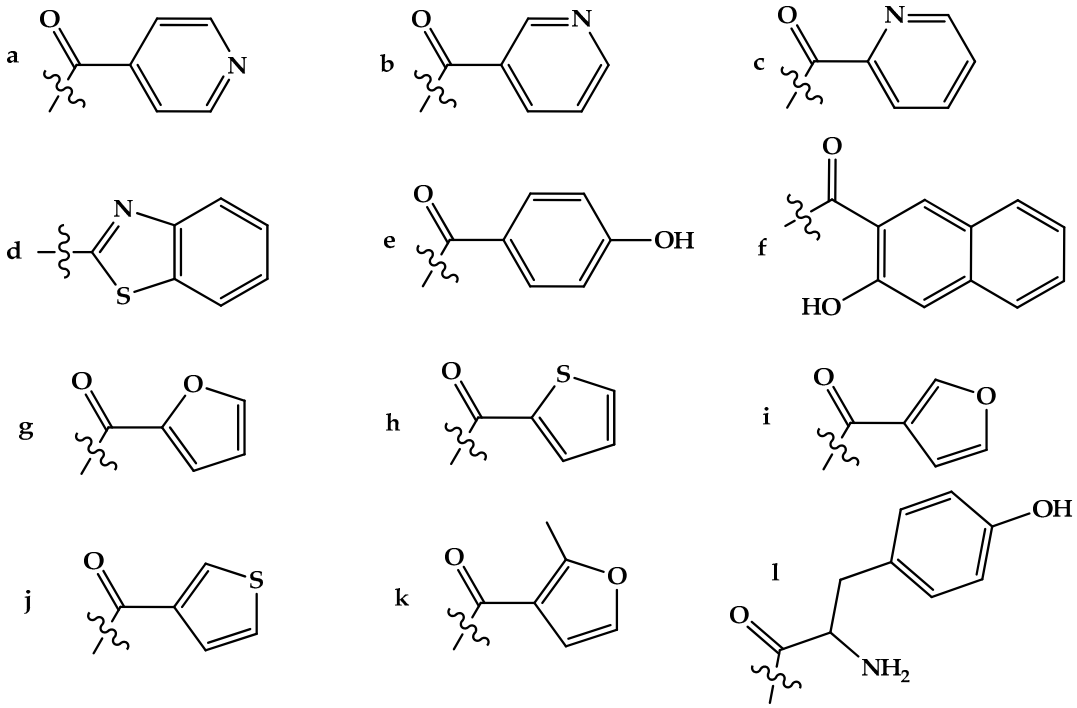

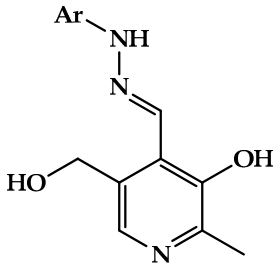

2a,g-j

Ar:

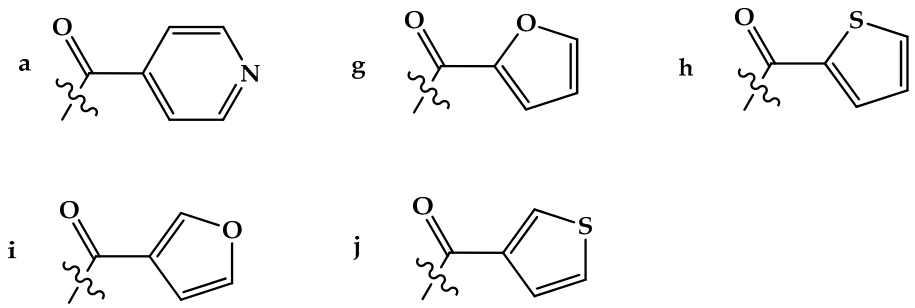

Figure 1. *Cont.*

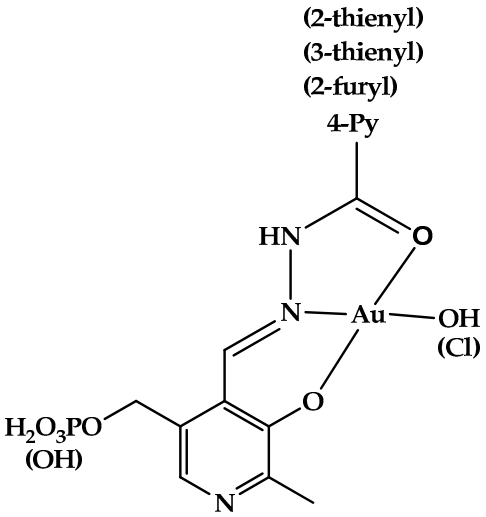

Figure 1. Structure of hydrazones derived from pyridoxal 5′-phosphate (**1a-l**) and pyridoxal (**2a**,**g–j**). Structure of gold(III) complexes **3**(**4**)**a**, **g**, **h**, **j** (the more detailed structural information about the complexes is available from the results of quantum chemical calculations [66]).

2. Results and Discussion

2.1. Structural Elucidation of Gold(III) Complexes

In general, the difference between the NMR spectra of hydrazones and their gold(III) complexes is evident from Figures S1 and S2. Comparison of ^{1}H NMR of free ligands to those of the complexes (see Figure S1 for spectra and refer to Table 1 for numerical data) indicates complexation via imine nitrogen and phenolic oxygen in site 3 of pyridoxal or pyridoxal 5-phosphate residue, as the protons of –NH–, –CH=, and –OH groups are deshielded upon complexation.

Probably, during the formation of Au–O and Au–N coordination bonds, the electron density is redistributed from the hydrazone to the metal ion, which leads to the deshielding of O–H and N–H protons (Table 1). In addition, this coordination geometry of gold(III) complexes was confirmed by us earlier using DFT methods [66]. In general, the coordination of ligands to gold(III) cation through N,O-donor atoms is typical, as shown in many papers (see, e.g., a review [67] or the recent detailed theoretical study of Au^{3+}-catalyzed [3 + 2] cycloaddition reaction between (Z)-C,N-diphenylnitrone and nitroethene [68]).

Negligible changes in the chemical shift of the ^{31}P atom (Figure S2) allow us to neglect the possibility of complexation through the phosphate group. Otherwise, a downfield shift by several ppm would be observed, as our previous paper [69] shows in the example of a gallium(III) complex with the analogous hydrazone. Complex formation involving N, O-donor atoms, instead of the $–PO_3H_2$ group, is in line with our results of quantum chemical calculations [66].

IR spectra (Figure S3, Table S1) of the complexes in comparison to those of free ligands also confirm complex formation as the stretching vibration of C=O bond are localized in the range of lower wavenumbers (**3a**: 1666 cm^{-1} vs. 1669 cm^{-1} [70]; **3g**: 1641 cm^{-1} vs. 1690 cm^{-1}; **3h**: 1677 cm^{-1} vs. 1681 cm^{-1} [71]; **3j**: 1635 cm^{-1} vs. 1689 cm^{-1} [72]; **4a**: 1633 cm^{-1} vs. 1689 cm^{-1}; **4j**: 1648 cm^{-1} vs. 1677 cm^{-1} [73]). On the contrary, the bands related to –CH=N- and ≥C-OH vibrations shift to the higher wavenumbers (**3a**: 1564 and 1280 cm^{-1} vs. 1527 and 1223 cm^{-1} [70]; **3g**: 1271 cm^{-1} vs. 1238 cm^{-1}; **3h**: 1637 cm^{-1} vs. 1542 cm^{-1} [71]; **4j**: 1546 cm^{-1} vs. 1532 cm^{-1} [73]).

Table 1. NMR chemical shifts (ppm) of hydrazones **1(2)a, g, h, j** and their gold(III) complexes **3(4)a, g, h, j** with signal assignment (structures with atom numbering are given in Figure S1). Symbol "s" marks singlet, "d" marks doublet, "t" marks triplet, "dd" marks doublet of doublets. Spin coupling constants are provided in Section 3.1 with the same marks for different multiplets.

Nucleus	1a	3a	Nucleus	1g	3g	1h	3h	1j	3j
–NH–	12.97s	13.23s	–NH–	12.76s	13.05s	12.82s	13.03s	12.60s	13.01s
–OH	12.28s	12.88s	–OH	12.30s	13.05s	12.33s	13.03s	12.40s	13.01s
H_6	8.89s	8.91s	H_6	8.87s	8.89s	8.83s	8.83s	8.81s	8.83s
$H_{11, 13}$	8.84d	8.91s	H_{11}	8.03s	8.08s	7.99d	8.02d	8.41d	8.02dd
H_7	8.03s	8.26s	H_7	8.01s	8.26s	8.02s	8.25s	8.01s	8.24s
$H_{10, 14}$	7.89d	7.96d	H_{13}	7.41d	7.46d	7.97d	8.02d	7.64d	7.31dd
			H_{12}	6.76d	6.80d	7.28t	7.32t	7.73dd	8.01d
$H_{5'}$	5.06d	5.20d	$H_{5'}$	5.05d	5.19d	5.06d	5.20d	5.05d	5.19d
$H_{2'}$	2.46s	2.61s	$H_{2'}$	2.44s	2.61s	2.45s	2.60s	2.45s	2.59s
^{31}P	−1.52s	−1.41s	^{31}P	−1.51s	−1.43s	−1.53s	−1.42s	−1.53s	−1.43s
Nucleus	**2a**	**4a**	**Nucleus**	**2g**	**4g**	**2h**	**4h**	**2j**	**4j**
–NH–	12.88s	13.04s	–NH–	12.97s	13.17s	12.97s	13.20s	13.06s	13.31s
–OH	13.30s	13.46s	–OH	13.07s	13.14s	13.15s	13.20s	12.94s	13.02s
H_6	9.07s	9.07s	H_6	8.99s	8.98s	8.99s	8.97s	8.98s	8.97s
$H_{11, 13}$	8.88d	8.96d	H_7	8.22s	8.28s	8.22s	8.29s	8.21s	8.29s
H_7	8.22s	8.31s	H_{11}	8.07s	8.08s	8.09d	8.08d	8.50s	8.50s
$H_{10, 14}$	7.97d	8.09d	H_{13}	7.50d	7.50d	8.02d	8.03d	7.75dd	7.76dd
			H_{12}	6.79d	6.80d	7.31t	7.32t	7.68dd	7.68dd
$H_{5'}$	4.77s	4.82s	$H_{5'}$	4.76s	4.79s	4.77s	4.81s	4.76s	4.80s
$H_{2'}$	2.60s	2.65s	$H_{2'}$	2.60s	2.64s	2.60s	2.65s	2.60s	2.65s

Therefore, the ^1H, ^{31}P NMR, and IR spectra confirm that the complexes of gold(III) with hydrazones are formed due to the interactions between metal cation and N, O-donor atoms of the ligand, as the most significant displacement is observed for proton signals of –CH=, –NH– and –OH groups, while the wavenumber of the C=O fragment is also altered significantly. In addition, mass spectra (Figure S4) confirm the successful synthesis and stoichiometric composition of the complex, viz., gold to ligand ratio of 1:1.

It is worth briefly discussing the differences in hydrazones and their complex structures reflected by the ^1H NMR spectra. The phosphate group introduced in molecules or complexes causes the most pronounced changes as the signal of the methylene group shifts downfield from ~4.8 to ~5.1 ppm and becomes split because of spin-coupling of protons with ^{31}P nuclei. The substitution of heteroatom from O to S (compare **1-4g** and **1-4h**, Figure S1) leads to a significant downfield shift in H_{13} (β-proton located next to C–C(=O) fragment) and H_{12} (another β-proton) from ~7.4 to ~8.0 ppm and ~6.8 to ~7.3 ppm, respectively. This deshielding is a consequence of the higher aromaticity of thiophene compared to that of the furan cycle. Finally, in the spectra of regioisomers **1-4h** and **1-4j**, the signals from H_{12} and H_{13} are mutually swapped as H_{12} deshields strongly from ~7.3 to ~7.8 ppm because of the neighboring sulfur atom (in **1-4j**), while the resonance of H_{13} moves upfield from ~8.0 to ~7.6 ppm. The proton signal of the hydrazone bridge (H_7, –CH=N–NH–) is almost insensitive to the nature of the aroyl substituent, and the differences in H_7 chemical shifts are also negligible between pyridoxal and pyridoxal 5′-phosphate derivatives. The same applies to the signal of proton H_6 belonging to the pyridoxal or pyridoxal 5′-phosphate residue. The resonance of H_6 weakly depends on substituents, as they are distant from this nucleus.

2.2. Cytotoxicity of Hydrazones **1a-l**

The IC50 (concentration leading to 50% mortality of the cells) values of hydrazones **1a-l** determined via MTT on two cell lines, colon cancer HCT116 and non-tumor human embryonic kidney HEK293T, are given in Table 2. The primary experimental data (titrations of different hydrazones vs. the standard drug, doxorubicin) can be found in Figure S5. The following IC50 values were obtained for the control drug: 0.07 ± 0.03 μM for HEK293T and 0.3 ± 0.8 μM for HCT116. Errors in Table 2 are the standard deviations obtained from logistic curve fitting.

Table 2. IC50 values (μM) ± SD of **1a-l** hydrazones determined for HCT116 and HEK293T cell lines.

Cell Line	1a	1b	1c	1d	1e	1f	1g	1h	1i	1j	1k	1l
HEK293T	>50	16 ± 3	16 ± 3	4 ± 2	32 ± 2	13 ± 4	21 ± 2	18 ± 2	27 ± 2	41 ± 4	10 ± 3	10 ± 7
HCT116	>50	17 ± 2	16 ± 2	6 ± 3	27 ± 5	22 ± 3	12 ± 2	12 ± 2	26 ± 6	42 ± 11	7 ± 3	9 ± 7

The data in Table 2 were used to build a simplistic model, which links such molecular descriptors as molecular weight (*MW*), molecular volume (*MV*), and polarizable surface area (*PSA*) with the IC50 values (see Table S2 containing the values adopted from Molinspiration software (https://www.molinspiration.com/) [74]). The log *P* (decimal logarithm of the partition coefficient between organic and aqueous phases characterizing the lipophilicity of compounds) was initially also used but was found to contribute negligibly. The correlation between the experimental and calculated results is relatively poor (Figure S6), which can be the consequence of a small dataset.

The linear Equations (1) and (2) for HEK293T and HCT116, respectively, with the LSQ-optimized coefficients, are used to obtain the calculated IC50 values:

$$1.0(\pm 0.3)MW + 0.5(\pm 0.2)PSA - 1.5(\pm 0.5)MV = IC50 \quad (1)$$

$$-0.4(\pm 0.5)MW + 0.1(\pm 0.3)PSA + 0.4(\pm 0.6)MV = IC50 \quad (2)$$

The regression coefficients in Equation (2) are insignificant as SDs exceed them in absolute value. As expected, the coefficients related to the molecular weight and volume are strongly negatively correlated (Pearson's correlations are of −0.98 value). It should be underlined that the linear model is too simple and may not reflect the more complex links between various descriptors. In addition, the descriptor set is too limited. However, because of a small dataset, expanding descriptors may not make sense.

In general, it can be noted that the hydrazones under study show no preference for cancer cells over the non-tumor ones, being almost equally toxic for both studied cultures. The most cytotoxic compound, **1d**, differs from others as it lacks a carbonyl group between hydrazide and heteroaromatic residues. Regioisomers **1b** and **1c** show the same IC50 values, while the derivative of isoniazid is similar in terms of cytotoxicity to the hydrazone containing the pyrazine carbohydrazide moiety [75], with IC50 for both compounds being more than 50 μM. The hydrazones containing five-membered heterocycles (**1g-j**) show some dependence on heteroatom position, with 2-substituted furyl (**1g**) and thienyl (**1h**) being more toxic than the 3-substituted ones (**1i**, **j**). Interestingly, the methyl group in position 2 of the 3-furyl cycle (**1k**) increases the cytotoxicity.

It is worth noting that the cytotoxicity of hydrazones reported in this contribution is comparable (or higher) with that reported by other authors who studied the hydrazones of various structures. For example, in paper [76], a library of 34 hydrazones containing different six- and five-membered aromatic substituents was collected, and only one, a derivative of bis-fluorinated benzoyl hydrazide, showed a notable toxic action towards the HCT116

cell line. A recent report [77] also presents a library of 34 hydrazones derived from benzothiazole and cyclobut-3-ene-1,2-dione with moderate toxic activity against the HCT116 cell line. No toxicity of substituted 1-benzylidene-2-phenylhydrazines was observed towards the HEK293T cell line by Alina Ghinet and co-workers [78]. The hydrazone derivatives of isoniazid containing the sulfonyl moiety were also at best moderately cytotoxic against HEK293T [79]. Taking into account the results obtained for various pyridoxal 5′-phosphate derivatives (**1a-l**), we can suggest that, in general, the hydrazone scaffold is not a suitable base for anticancer drugs.

2.3. Antibacterial Activity of Hydrazones and Their Gold(III) Complexes

The values of the diameter of the zone of bacterial and fungal growth inhibition are given in Table 3. Some examples of primary experimental data (Petri dishes) can be found in Figure S7.

Table 3. Diameters of growth inhibition (nm) zones caused by gold(III) complexes with hydrazones. Standard deviation of zone diameter measurements does not exceed ±1 mm.

Compound	Concentration, μg mL^{-1}	Microorganism					pH
		S. aureus INA 00985	*B. subtilis* ATCC 6633	*E. coli* ATCC 25922	*P. aeruginosa* ATCC 27853	*C. albicans* ATCC 14053	
$[HAuCl_4]$	10	50	40	40	42	30	1
	1	35	24	24	25	17	
3a	5	no effect	no effect	no effect	no effect	no effect	8
	1	no effect	no effect	no effect	no effect	no effect	
3g	5	20	15	15	18	13	8
	1	12	11	13	13	no effect	
3h	5	12	no effect	11	10	no effect	6
	1	no effect	no effect	no effect	no effect	no effect	8
3j	5	25	20	20	24	18	6
	1	15	13	15	18	11	8
4a	5	no effect	no effect	no effect	no effect	no effect	7
	1	no effect	no effect	no effect	no effect	no effect	8
4g	5	17	13	16	15	no effect	8
	1	11	no effect	12	12	no effect	8
4h	5	11	no effect	11	11	no effect	7
	1	no effect	no effect	no effect	no effect	no effect	8
4j	5	12	no effect	10	no effect	no effect	7
	1	no effect	no effect	no effect	no effect	no effect	8
Mixtures of $[HAuCl_4]$ and hydrazones solutions in 0.025 M Tris-HCl buffer							
$[HAuCl_4]$ + **1a**	10	22	16	23	24	14	
	1	22	14	20	22	no effect	7
$[HAuCl_4]$ + **1g**	10	24	15	23	25	14	
	1	22	13	18	22	no effect	7
$[HAuCl_4]$ + **1h**	10	28	20	25	25	15	
	1	22	12	16	25	no effect	7
$[HAuCl_4]$ + **1i**	10	17	no effect	17	16	no effect	
	1	22	14	18	24	no effect	7
$[HAuCl_4]$ + **1j**	10	25	20	24	25	15	
	1	22	15	20	25	no effect	7
$[HAuCl_4]$ + **2a**	10	18	no effect	15	15	no effect	
	1	20	12	20	25	no effect	7
$[HAuCl_4]$ + **2g**	10	27	17	23	25	15	
	1	22	12	18	24	no effect	7
$[HAuCl_4]$ + **2h**	10	15	no effect	16	18	no effect	
	1	22	12	15	25	no effect	7
$[HAuCl_4]$ + **2i**	10	25	20	25	25	15	
	1	22	13	20	25	no effect	7
$[HAuCl_4]$ + **2j**	10	18	no effect	15	15	no effect	
	1	22	13	18	25	no effect	7

Hydrazones **1**,**2a**, **g-j** show no antibacterial effect (see Figure S7a–h). Gold(III) complexes of the hydrazones **3**,**4a**, **g**, **h**, **j** possess some activity towards both Gram-positive and Gram-negative strains, which is comparable to the available literature data (especially

for copper(II) complexes) [80,81]. Interestingly, some complexes formed by hydrazones derived from pyridoxal 5′-phosphate are also active against the yeast *C. albicans*, while no complex containing a pyridoxal-derived ligand inhibits fungal growth. The 0.025 M Tris-HCl buffer (pH 8.5) used as a solvent for hydrazones and complexes has neither antibacterial nor antifungal activity.

The antibacterial effect of gold complexes is attributed to various factors, including the degree of oxidation of gold, the structure of the ligands, and the characteristics of the bacterial cell membrane [82]. The type of ligands attached to the gold ion can significantly influence the stability, solubility, and ability of the complex to interact with bacterial targets. As we have demonstrated, the vitamin B_6 hydrazones considered in this study do not exhibit antibacterial activity. We believe that the low cytotoxicity and antibacterial activity of free hydrazones are related to the aldehyde part of the molecule, as it is a vitamin. The formation of complexes with gold(III) enhances the antibacterial activity of these ligands, although it does not reach the level of effective drugs. Additionally, the polar structure of the complexes may hinder their penetration through the bacterial cell membrane.

While testing the mixtures of the 0.025 M Tris-HCl buffered solutions containing [$HAuCl_4$] and hydrazones (Table 2), we expected that the antimicrobial activity of these solutions would be roughly the same as that characterizing the synthesized gold(III) complexes. However, all these mixture were observed to have antimicrobial effects (Table 3, Figure S8, inhibited growth zone diameters varied from 12 to 25 mm) similar to that of the control, which was a solution of [$HAuCl_4$] in the same Tris-HCl buffer without hydrazones (Figure S9; the diameters of growth inhibition zone caused by [$HAuCl_4$] were 15 to 25 mm). Therefore, the hydrazones added to gold(III) solution do not provide the metal with any additional antimicrobial activity. They are possibly unable to form the complexes with gold(III) in neutral solution containing a relatively large concentration of Tris (0.025 M).

3. Materials and Methods

3.1. Chemicals

Synthesis of hydrazones as well as their spectral properties are described elsewhere for compounds **1a-c** [70], **1d** [83], **1e**, **f**, **l** [84], **1g**, **h** [85], **1i**, **j** [72], **1k** [86], and **2a**, **g-j** [73].

Gold(III) complexes **3**, **4a**, **g**, **h**, **j** were synthesized according to the following general procedure (Figure 2): 0.35 mmol (mass depends on molecular weight) of every hydrazone (**1**, **2a**, **e**, **g**, **h**, **j**) was dissolved in 10 mL of ethanol containing one drop of triethylamine (to ensure complete solubility) and heated to 60 °C. To this solution, a solution of 110 mg (0.35 mmol) of [$HAuCl_4$] in 5 mL of ethanol was added dropwise. The resulting mixture was stirred under reflux at 60 °C for 3 h. The precipitate formed was filtered off and dried in air. The complexes obtained were characterized using ^{1}H, ^{31}P NMR, IR, and mass spectral analysis (Figures S1–S4, respectively). Atom numbering used for NMR signal assignment can be found in Figure S1. NMR spectra of the free ligands registered for comparison are also provided (Figures S1 and S2).

Complex **3a**. Red brownish crystals. Yield 100.6 mg (58.9%). M_z 597.70 (calcd. 597.68 for [AuClL]$^-$). Elemental, exp (calcd.): C 29.98 (30.14), H 2.84 (2.70), N 7.13 (7.03), O 16.64 (16.06). IR(KBr), cm^{-1}: 3423s, 2918vs, 2848s, 1666s, 1564s, 1486m, 1411m, 1380m, 1280vs, 1180s, 1091s, 1016s, 927s (here and below in IR spectra, “vs” means “very strong”, “s” means “strong”, “m” means “medium”, and “w” means “weak”). ^{1}H NMR (500.17 MHz), δ, ppm (DMSO-*d6*): 13.23s (1H, -NH-), 12.88s (1H, -OH), 8.91s (3H, H_6, $H_{11,13}$), 8.26s (1H, H_7), 7.96d (^{3}J = 5.4 Hz, 2H, $H_{10,14}$), 5.20d (^{3}J = 9.0 Hz, 2H, $H_{5'}$), 2.61s (3H, $H_{2'}$). ^{31}P NMR (202.47 MHz), δ, ppm (DMSO-*d6*): −1.41s.

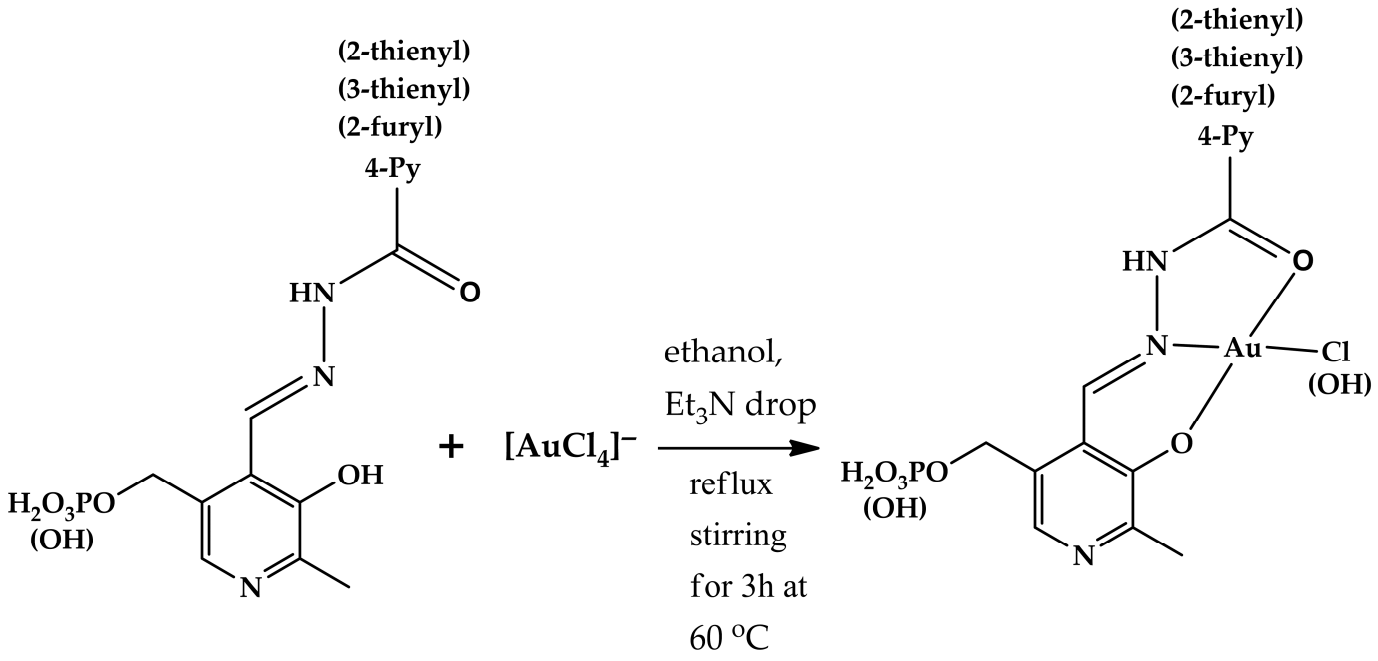

Figure 2. Scheme of synthesis of gold(III) complexes with hydrazones derived from pyridoxal and pyridoxal 5′-phosphate.

Complex **3g**. Red brownish crystals. Yield 87.3 mg (50.2%). M_z 567.89 (calcd. 568.02 for $[AuOHL]^-$). Elemental, exp (calcd.): C 29.71 (29.59), H 2.73 (2.84), N 5.01 (4.93), O 22.89 (22.53). IR(KBr), cm^{-1}: 3427vs, 2922s, 2854s, 1641s, 1471s, 1384s, 1271s, 1184s, 1101m, 1051m, 920m. ^1H NMR (500.17 MHz), δ, ppm (DMSO-*d6*): 13.05s (2H, -NH-, -OH), 8.89s (1H, H_6), 8.26s (1H, H_7), 8.08s (1H, H_{11}), 7.46d (^3J = 3.5 Hz, 1H, H_{13}), 6.80d (^3J = 3.5 Hz, 1H, H_{12}), 5.19d (^3J = 9.0 Hz, 2H, $H_{5'}$), 2.61s (3H, $H_{2'}$). ^{31}P NMR (202.47 MHz), δ, ppm (DMSO-*d6*): −1.43s.

Complex **3h**. Red brownish crystals. Yield: 95.0 mg (55.2%). M_z 584.20 (calcd. 584.27 for $[AuOHL]^-$). Elemental, exp (calcd.): C 28.87 (28.78), H 2.69 (2.76), N 4.73 (4.79), O 19.44 (19.17), S 5.55 (5.49). IR(KBr), cm^{-1}: 3431vs, 2920s, 2850s, 1677s, 1637s, 1537s, 1475m, 1417m, 1384s, 1261vs, 1184vs, 1076vs, 925s. ^1H NMR (500.17 MHz), δ, ppm (DMSO-*d6*): 13.03s (2H, -NH-, -OH), 8.83s (1H, H_6), 8.25s (1H, H_7), 8.02d (^3J = 5.1 Hz, 1H, H_{11}), 8.01d (^3J = 3.5 Hz, 1H, H_{13}), 7.32t (^3J = 4.3 Hz, 1H, H_{12}), 5.20d (^3J = 9.1 Hz, 2H, $H_{5'}$), 2.60s (3H, $H_{2'}$). ^{31}P NMR (202.47 MHz), δ, ppm (DMSO-*d6*): −1.42s.

Complex **3j**. Red brownish crystals. Yield: 111.7 mg (64.9%). M_z 584.28 (calcd. 584.27 for $[AuOHL]^-$). Elemental, exp (calcd.): C 28.94 (28.78), H 2.61 (2.76), N 4.75 (4.79), O 19.52 (19.17), S 5.38 (5.49). IR(KBr), cm^{-1}: 3423vs, 2919s, 2852m, 1635s, 1533m, 1469m, 1384s, 1263s, 1197s, 1074s, 923w. ^1H NMR (500.17 MHz), δ, ppm (DMSO-*d6*): 13.01s (2H, -NH-, -OH), 8.83s (1H, H_6), 8.24s (1H, H_7), 8.02d (^3J = 5.0 Hz, 1H, H_{11}), 8.01d (^3J = 3.8 Hz, 1H, H_{12}), 7.31dd (^3J = 4.3 Hz, ^4J = 4.1 Hz, 1H, H_{13}), 5.19d (^3J = 9.1 Hz, 2H, $H_{5'}$), 2.59s (3H, $H_{2'}$). ^{31}P NMR (202.47 MHz), δ, ppm (DMSO-*d6*): −1.43s.

Complex **4a**. Red brownish crystals. Yield: 61.9 mg (33.2%). M_z 500.46 (calcd. 500.26 for [AuOHL]). Elemental, exp (calcd.): C 35.88 (36.08), H 3.02 (3.23), N 8.57 (8.42), O 13.10 (12.82). IR(KBr), cm^{-1}: 3454vs, 2919m, 2850m, 1633s, 1544s, 1415s, 1274s, 1164s, 1072s, 1031m, 844m. ^1H NMR (500.17 MHz), δ, ppm (DMSO-*d6*): 13.46s (1H, -OH), 13.04s (1H, -NH-), 9.07s (1H, H_6), 8.96d (^3J = 5.5 Hz, 2H, $H_{11,13}$), 8.31s (1H, H_7), 8.09d (^3J = 5.5 Hz, 2H, $H_{10,14}$), 4.82s (2H, $H_{5'}$), 2.65 s (3H, $H_{2'}$).

Complex 4**g**. Red brownish crystals. Yield: 45.8 mg (23.3%). M_z 504.81 (calcd. 504.67 for [AuClL]). Elemental, exp (calcd.): C 33.25 (33.32), H 2.28 (2.40), N 5.76 (5.55), O 12.94

(12.68). IR(KBr), cm^{-1}: 3427vs, 2922s, 2854s, 1641s, 1471s, 1384s, 1271s, 1184s, 1101m, 1051m, 920m. ^1H NMR (500.17 MHz), δ, ppm (DMSO-*d6*): 13.17s (1H, -NH-), 13.14s (1H, -OH), 8.98s (1H, H_6), 8.28s (1H, H_7), 8.08s (1H, H_{11}), 7.51d (^3J = 3.4 Hz, 1H, H_{13}), 6.80d (^3J = 3.4 Hz, 1H, H_{12}), 4.79s (2H, $H_{5'}$), 2.64s (3H, $H_{2'}$).

Complex **4h**. Red brownish crystals. Yield: 17.8 mg (9.3%). M_z 505.35 (calcd. 505.29 for [AuOHL]). Elemental, exp (calcd.): C 33.39 (33.34), H 2.84 (3.00), N 5.42 (5.55), O 12.88 (12.69), S 6.29 (6.36). IR(Br), cm^{-1}: 3448s, 2926w, 2850w, 1683s, 1621s, 1544s, 1473s, 1427m, 1380m, 1353m, 1270vs, 1155s, 1101m, 1066m, 1031m, 846m. ^1H NMR (500.17 MHz), δ, ppm (DMSO-*d6*): 13.20s (2H, -OH, -NH-), 8.97s (1H, H_6), 8.29s (1H, H_7), 8.08d (^3J = 4.3 Hz, 1H, H_{11}), 8.03d (^3J = 4.3 Hz, 1H, H_{13}), 7.32t (^3J = 4.3 Hz, 1H, H_{12}), 4.81s (2H, $H_{5'}$), 2.65s (3H, $H_{2'}$).

Complex **4j**. Red brownish crystals. Yield: 87.7 mg (45.8%). M_z 523.33 (calcd. 523.29 for [AuClL]). Elemental, exp (calcd.): C 32.23 (32.17), H 2.56 (2.70), N 5.24 (5.36), O 9.43 (9.18), S 6.15 (6.16). IR(Br), cm^{-1}: 3454vs, 2919vs, 2850s, 1648s, 1546vs, 1469s, 1411s, 1303m, 1263vs, 1214s, 1162s, 1095m, 1025s, 852s. ^1H NMR (500.17 MHz), δ, ppm (DMSO-*d6*): 13.31s (1H, -NH-), 13.02s (1H, -OH), 8.97s (1H, H_6), 8.50d (^4J = 0.6 Hz, 1H, H_{11}), 8.29s (1H, H_7), 7.76d (^3J = 7.7 Hz, 1H, H_{12}), 7.68d (^3J = 4.9 Hz, 1H, H_{13}), 4.80s (2H, $H_{5'}$), 2.65s (3H, $H_{2'}$).

NMR spectra (Figures S1 and S2) are almost free from signals of impurities, which confirms the success of the synthesis.

3.2. Spectrometers

IR spectra were registered using a Thermo Nicolet Avatar 360 FTIR spectrometer (Thermo Fisher, MA, USA) with a range of 400–4000 cm^{-1}. The samples were prepared by dispersing them in KBr.

The Shimadzu Biotech Axima Confidence system (Shimadzu, CA, USA) was used to record MS (MALDI TOF) spectra. First, the solution of the matrix compound (either α-cyano-4-hydroxycinnamic or 2,5-dihydroxybenzoic acid) was applied to the plate. Next, the solution of the studied complex in ethanol was applied to the plate above and allowed to dry in air before analysis.

^1H, ^{31}P NMR spectra were recorded using a Bruker Avance III 500 NMR spectrometer (Bruker, Karlsruhe, Germany) with ^1H, ^{31}P operating frequencies of 500.17 and 202.47 MHz, respectively. Temperature control (298 K) was achieved using a Bruker variable temperature unit (BVT-2000, Bruker, Karlsruhe, Germany). Chemical shifts were determined relative to the external standard, HMDSO (Sigma Aldrich, Darmstadt, Germany) and 85% phosphoric acid (Sigma Aldrich, Darmstadt, Germany), with an error of $\pm$0.01 ppm. The standard pulse sequence [87] from TopSpin 3.6.1 software was used to record the spectra.

The elemental analysis (C, H, N, O, S) of gold(III) complexes with hydrazones was performed using a FLASH EA1112 setup (Termo Quest, Rodano, Italy).

3.3. Cells

Tumor and non-tumor cells were used as the model lines for biological experiments: HCT116 (human colon adenocarcinoma) and HEK293T (human embryonal kidney, non-tumor cells). Both lines were obtained from the American Type Culture Collection (ATCC, Manassas, VA, USA). Cells were grown in DMEM (PanEco, Moscow, Russia) supplemented with 10% fetal bovine serum (Biosera, Cholet, France), penicillin-streptomycin mix (100 U/mL and 100 μg/mL, respectively), and 2 mM L-glutamine (PanEco, Moscow, Russia), in a humidified atmosphere (37 °C in 5% CO_2).

3.4. MTT Assay

To measure the potential cytotoxicity effect of hydrazones **1a-l** on living cells, the MTT test was used. To reach a high stock concentration, all hydrazones derived from pyridoxal 5′-phophate were dissolved in 1.5 M TRIS-HCl, pH 8.8. Cells were seeded in 96-well plates

at a density of 5000 cells per well and incubated overnight (37 °C in 5% CO_2). The next day, hydrazone solutions were added to cells at increased concentration (ranging from 0.097 μM to 50 μM with an increase of 2 times in each step), and then cells were incubated for 72 h. In a separate set of wells, doxorubicin was also added to cells at an increased concentration as a control. After incubation, 5 mg/mL MTT reagent (3-(4,5-dimethylthiazol-2-yl)-2,5-diphenyltetrazolium bromide; Dia-M, Moscow, Russia) was added to each well, and the cells were incubated for 3 h. The supernatant was then decanted, and 100 μL DMSO (PanEco, Moscow, Russia) was added to each well to dissolve the formazan crystals formed. Colorimetric measurements were made at λ = 570 nm using a CLARIOstar Plus microplate reader (BMG LABTECH, Ortenberg, Germany). Each compound was tested by the MTT test at least 3 times.

3.5. Antibacterial Assay

The antimicrobial action of complexes **3**, **4a**, **g**, **h**, **j,** as well as the mixtures of [$HAuCl_4$] and hydrazones **1**, **2a**, **g-j,** was tested using a disk diffusion method (diffusion of the test compound into agar inhibiting the growth of test cultures). *S. aureus* INA 00985, *B. subtilis* ATCC 6633 (Gram-positive bacteria), *E. coli* ATCC 27853, *P. aeruginosa* ATCC 27,853 (Gram-negative bacteria), and *C. albicans* ATCC 14,053 (yeast) were inoculated on meat peptone agar and placed in Petri dishes. Solutions of complexes or mixtures of hydrazones and [$HAuCl_4$] in aqueous 0.025 M Tris-HCl buffer (pH 8) were applied to 5 mm pits in the medium. After one day of incubation in the thermostat at 37 °C, the diameters of growth inhibition zones were measured. Two concentrations of each complex or mixture component were tested: 10 or 5, and 1 μg mL^{-1}. The effect of the 0.025 M Tris-HCl buffer itself or a buffered aqueous solution of [$HAuCl_4$] was also evaluated in the blank experiment.

3.6. Theory

A simple chemometric model linking the IC50 values determined by MTT to molecular descriptors such as molecular weight, polarizable surface area, and molecular volume was built in analogy with the previously described one [73]. The only difference is introducing the weight matrix to take into account the standard deviations determined for IC50 values.

4. Conclusions

Eight novel gold(III) complexes with pyridoxal and pyridoxal 5′-phosphate-derived hydrazones were synthesized and characterized using various spectroscopic techniques. Cation interacts with ligand through imine nitrogen and phenolic oxygen, as well as carbonyl group, as it was shown using ^{1}H, ^{31}P NMR, and IR spectroscopy. The phosphate group does not participate in complex formation.

The cytotoxic effect of several hydrazones derived from pyridoxal 5′-phosphate was studied using both tumor (HCT116) and immortalized (HEK293T) cell lines. The hydrazones proved to be less toxic than the standard drug, doxorubicin (IC50 0.07 ± 0.03 μM for HEK293T and 0.3 ± 0.8 μM for HCT116), with the hydrazones' IC50 higher by one or two orders (4 to 50 or more μM) and showed no preference for the tumor cells over the non-tumor ones. Combined with the literature data on cytotoxicity obtained for analogous compounds, it can be suggested that hydrazones of various structures are not suitable candidates for antitumor drugs. There is no clear link between the bioactivity evaluated as IC50 and molecular descriptors such as molecular weight, polarizable surface area, and molecular volume, as the correlation coefficients of the respective linear regressions are quite small (0.3737 in the case of HCT116 and 0.5868 for HEK293T). The complexes of gold(III) with pyridoxal 5′-phosphate and pyridoxal-derived hydrazones were tested

as antibacterial compounds. Isoniazid derivatives were found to be completely ineffective, while the complexes with ligands containing five-membered heterocycles show some activity against both Gram-positive and Gram-negative bacteria and *C. albicans* (fungi), inhibiting the growth of microorganisms with a diameter of 10 to 24 mm. The mixtures of the solutions containing [$HAuCl_4$] and hydrazones were found to be no more efficient against bacteria and fungi (the diameters of inhibited growth zone varied from 12 to 25 mm) than a solution of [$HAuCl_4$] alone (which hindered the growth of bacteria within the range of diameters from 15 to 25 mm). The data obtained from this study will provide essential insights into databases focused on predicting the antibacterial and cytostatic activity of compounds, highlighting the significance of "negative results" in guiding future research and development efforts.

Supplementary Materials: The following supporting information can be downloaded at: https://www.mdpi.com/article/10.3390/inorganics13100335/s1. Figure S1: ^{1}H NMR spectra (DMSO-d6, 500.17 MHz) of: (a) **1a** (top) and **3a** (bottom); (b) **1g** (top) and **3g** (bottom); (c) **1h** (top) and **3h** (bottom); (d) **1j** (top) and **3j** (bottom); (e) **2a** (top) and **4a** (bottom); (f) **2g** (top) and **4g** (bottom); (g) **2h** (top) and **4h** (bottom); (h) **2j** (top) and **4j** (bottom); Figure S2: ^{31}P NMR spectra (DMSO-d6, 202.47 MHz) of: (a) **1a** (top) and **3a** (bottom); (b) **1g** (top) and **3g** (bottom); (c) **1h** (top) and **3h** (bottom); (d) **1j** (top) and **3j** (bottom); Figure S3: IR spectra of gold(III) complexes with pyridoxal 5′-phosphate or pyridoxal-derived hydrazones: (a) **3a**; (b) **3g**; (c) **3h**; (d) **3j**; (e) **4a**; (f) **4g**; (g) **4h**; (h) **4j** in KBr matrix; Table S1: The most important bands in IR spectra of gold(III) complexes **3**(**4**)**a**, **g**, **h**, **j** with hydrazones assigned; Figure S4: MALDI TOF mass spectra of gold(III) complexes with pyridoxal 5′-phosphate or pyridoxal-derived hydrazones: (a) **3a**; (b) **3g**; (c) **3h**; (d) **3j**; (e) **4a**; (f) **4g**; (g) **4h**; (h) **4j**. The following matrices were used: α-cyano-4-hydroxycinnamic acid (a–f), 2,5-dihydroxybensoic acid (g,h); Figure S5: Survivability of: (a–l) HEK293T; (m–x) HCT116 cells determined in MTT upon addition of different hydrazones **1a–l** taken in different concentrations. IC50 values are determined from these graphs using LSQ method from the best fit by logistic curve; Table S2: Molecular weight, polarizable surface are and molecular volume of hydrazones **1a–l**; Figure S6: Correspondence between the experimental and modeled IC50 values for: (a) HEK293T; (b) HCT116 cells; Figure S7: Petri dishes containing *P. aeruginosa* (a–d, u–x), *C. albicans* (e–h, y–ab), *S. aureus* (i–l), *B. subtilis* (m–p), *E. coli* (q–t) affected by tetrachloroaurate(III), hydrazones **1**,**2a**, **g**, **h**, **j** and complexes **3**,**4a**, **g**, **h**, **j**. Numbers correspond to the following compounds: 1—[$HAuCl_4$]; 2–**1a**; 3—**2a**; 4—**1g**; 5—**2g**; 6—**1h**; 7—**2h**; 8—**1i**; 9—**2i**; 10—**1j**; 11—**2j**; 12—**3a**; 13—**4a**; 14—**3g**; 15—**4g**; 16—**3h**; 17—**4h**; 18—**3j**; 19—**4j**. Concentrations of the hydrazones or gold(III) complexes: (a,b,e,f,i,k,m,o,q,s,u,w,y), aa—1 μg mL^{-1}; (c,d,g,h) 10 μg mL^{-1}; (j,l,n,p,r,t,v,x,z), ab—5 μg mL^{-1}; Figure S8: Petri dishes containing *S. aureus* (a-d), *B. subtilis* (e-h), *E. coli* (i-l), *P. aeruginosa* (k-o), *C. albicans* (p-s), affected by the mixtures of tetrachloroaurate(III) and hydrazones **1**,**2a**, **g**, **h**, **j** solutions. Numbers correspond to the following mixtures: 1, 11—[$HAuCl_4$] + **1a**; 2, 12—[$HAuCl_4$] + **1g**; 3, 13—[$HAuCl_4$] + **1h**; 4, 14—[$HAuCl_4$] + **1i**; 5, 15—[$HAuCl_4$] + **1j**; 6, 16—[$HAuCl_4$] + **2a**; 7, 17—[$HAuCl_4$] + **2g**; 8, 18—[$HAuCl_4$] + **2h**; 9, 19—[$HAuCl_4$] + **2i**; 10, 20—[$HAuCl_4$] + 2**j**. Concentrations of tetrachloroaurate(III) and hydrazones: (a,b,e,f,i,j,m,n,q,r) each 10 μg mL^{-1}; (c,d,g,h,k,l,o,p,s,t) each 1 μg mL^{-1}; Figure S9: Control experiment carried out with [$HAuCl_4$] dissolved in Tris-HCl buffer (pH 8.5): (a) *S. aureus*: gold(III) concentration 1 μg mL^{-1} (left), 10 μg mL^{-1} (right); (b) *B. subtilis*: gold(III) concentration 1 μg mL^{-1} (left), 10 μg mL^{-1} (right); (c) *E. coli*: gold(III) concentration 10 μg mL^{-1} (left), 1 μg mL^{-1} (right); (d) *P. aeruginosa*: gold(III) concentration 10 μg mL^{-1} (left), 1 μg mL^{-1} (right); (e) *C. albicans*: gold(III) concentration 10 μg mL^{-1} (left), 1 μg mL^{-1} (right).

Author Contributions: Conceptualization, G.A.G. and V.S.S.; methodology, G.A.G., A.K.I., O.N.S., and V.S.S.; software, G.A.G. and A.K.I.; validation, D.V.P., M.N.Z., and V.S.S.; formal analysis, D.V.P. and G.A.G.; investigation, D.V.P., A.K.I., O.N.S., and M.N.Z.; resources, D.V.P. and V.S.S.; data curation, A.K.I. and G.A.G.; writing—original draft preparation, A.K.I., M.N.Z., and G.A.G.; writing—review and editing, G.A.G. and V.S.S.; visualization, A.K.I. and O.N.S.; supervision, G.A.G. and V.S.S.;

project administration, G.A.G.; funding acquisition, G.A.G. All authors have read and agreed to the published version of the manuscript.

Funding: This research was funded by the Russian Science Foundation, grant number 22-73-10009-P, https://rscf.ru/project/22-73-10009-P/, accessed on 11 October 2025. The work of Sineva O.N. and Sadykova V.S. was carried out as part of institutional funding of the Gause Institute of New Antibiotics.

Institutional Review Board Statement: Not applicable.

Informed Consent Statement: Not applicable.

Data Availability Statement: The original contributions presented in the study are included in the article/Supplementary Material; further inquiries can be directed to the corresponding author.

Acknowledgments: The authors would like to thank the Center for Precision Genome Editing and Genetic Technologies for Biomedicine, a division of the Institute of Gene Biology, Russian Academy of Science, for providing the CLARIOStar Plus microplate reader.

Conflicts of Interest: The authors declare no conflicts of interest.

Abbreviations

The following abbreviations are used in this manuscript:

LSQ	Least Squares Method
MW	Molecular Weight
MV	Molecular Volume
PSA	Polarizable Surface Area
INA	Institute of New Antibiotics
ATCC	American Type Culture Collection
DMEM	Dulbecco's Modified Eagle Medium
MALDI TOF	matrix-assisted laser desorption/ionization time-of-flight
HMDSO	hexamethyldisiloxane

References

1. World Health Organization. Global Cancer Burden Growing, amidst Mounting Need for Services. Available online: https://www.who.int/news/item/01-02-2024-global-cancer-burden-growing{-}{-}amidst-mounting-need-for-services (accessed on 15 October 2024).
2. Teng, J.; Imani, S.; Zhou, A.; Zhao, Y.; Du, L.; Deng, S.; Li, J.; Wang, Q. Combatting Resistance: Understanding Multi-Drug Resistant Pathogens in Intensive Care Units. *Biomed. Pharmacother.* **2023**, *167*, 115564. [CrossRef]
3. Rollas, S.; Küçükgüzel, S.G. Biological Activities of Hydrazone Derivatives. *Molecules* **2007**, *12*, 1910–1939. [CrossRef]
4. Kargar, H.; Fallah-Mehrjardi, M.; Munawar, K.S. Metal Complexes Incorporating Tridentate ONO Pyridyl Hydrazone Schiff Base Ligands: Crystal Structure, Characterization and Applications. *Coord. Chem. Rev.* **2024**, *501*, 215587. [CrossRef]
5. Marzano, S.; Miglietta, G.; Morigi, R.; Marinello, J.; Arleo, A.; Procacci, M.; Locatelli, A.; Leoni, A.; Pagano, B.; Randazzo, A.; et al. Balancing Affinity, Selectivity, and Cytotoxicity of Hydrazone-Based G-Quadruplex Ligands for Activation of Interferon β Genes in Cancer Cells. *J. Med. Chem.* **2022**, *65*, 12055–12067. [CrossRef]
6. Alam, A.; Khan, F.; Rehman, N.U.; Zainab; Elhenawy, A.A.; Islam, W.U.; Ali, M.; Aziz, S.; Al-Harrasi, A.; Ahmad, M. Flurbiprofen Clubbed Schiff's Base Derivatives as Potent Anticancer Agents: In Vitro and In Silico Approach towards Breast Cancer. *J. Mol. Struct.* **2025**, *1321*, 139743. [CrossRef]
7. Deepa, S.; Mathangi, N.; Mudavath, R.; Shekhar, I.; Aparna, A.V.; Sarala Devi, C. Heteroleptic Complexes of Hydrazone Scaffold of Picolinoyl N- Oxide and 2,4 Dihydroxy Phenyl Moieties; Evaluation of Antioxidant Activity, DNA and Protein Binding Properties and in Vitro Antiproliferation Studies. *Inorganica Chim. Acta* **2025**, *574*, 122391. [CrossRef]
8. Firouzi, M.; Haghighijoo, Z.; Eskandari, M.; Mohabbati, M.; Miri, R.; Jamei, M.H.; Poustforoosh, A.; Nazari, S.; Firuzi, O.; Khoshneviszadeh, M.; et al. Synthesis and Cytotoxic Activity Evaluation of Novel Imidazopyridine Carbohydrazide Derivatives. *BMC Chem.* **2024**, *18*, 6. [CrossRef] [PubMed]
9. Schiavon, E.; Rezzola, S.; Filippi, E.; Turati, M.; Parrasia, S.; Bernardotto, S.; Stocco, M.; Szabò, I.; Mattarei, A.; Ronca, R.; et al. A Novel Mertansine Conjugate for Acid-Reversible Targeted Drug Delivery Validated through the Avidin-Nucleic-Acid-NanoASsembly Platform. *Nanomed. Nanotechnol. Biol. Med.* **2024**, *62*, 102784. [CrossRef] [PubMed]

10. Shakirova, O.G.; Morozova, T.D.; Kudyakova, Y.S.; Bazhin, D.N.; Kuratieva, N.V.; Klyushova, L.S.; Lavrov, A.N.; Lavrenova, L.G. Synthesis, Structure, and Properties of a Copper(II) Binuclear Complex Based on Trifluoromethyl Containing Bis(Pyrazolyl)Hydrazone. *IJMS* **2024**, *25*, 9414. [CrossRef]
11. Kadi, I.; Şekerci, G.; Boulebd, H.; Zebbiche, Z.; Tekin, S.; Benarous, K.; Serseg, T.; Küçükbay, F.; Küçükbay, H.; Boumoud, T. Exploring the Anticancer Potential of New 3-cyanopyridine Derivatives Bearing N-acylhydrazone Motif: Synthesis, DFT Calculations, Cytotoxic Evaluation, Molecular Modeling, and Antioxidant Properties. *J. Biochem. Mol. Toxicol.* **2024**, *38*, e23819. [CrossRef]
12. Tapera, M.; Doğan, E.; Şahin, K.; Gözkamane, G.A.; Kekeçmuhammed, H.; Sandal, S.; Gurkan, A.C.; Bora, R.E.; Anber, A.; Durdagi, S.; et al. Imidazole-Based Hydrazones as Potent Anti-Colon Cancer Agents: Design, Synthesis, Biological Evaluation and Computational Studies. *J. Mol. Struct.* **2024**, *1318*, 139240. [CrossRef]
13. Elgohary, M.K.; Elkotamy, M.S.; Al-Warhi, T.; Eldehna, W.M.; Abdel-Aziz, H.A. Development of New LSM-83177 Analogues as Anti-Tumor Agents against Colorectal Cancer Targeting P53-MDM2 Interaction. *Bioorganic Chem.* **2024**, *153*, 107766. [CrossRef] [PubMed]
14. Basu Baul, T.S.; Hlychho, B.; Das Pramanik, S.; Lyčka, A.; Roy, P.; Mahmoud, A.G.; Guedes Da Silva, M.F.C. Organotin(IV) Complexes Derived from 2,6-Diacetylpyridine Bis(2-Hydroxybenzoylhydrazone) as Prospective Anti-Proliferative Agents: Synthesis, Characterization, Structures and in Vitro Anticancer Activity. *J. Inorg. Biochem.* **2024**, *261*, 112693. [CrossRef] [PubMed]
15. Kumar, S.; Oh, J.M.; Prabhakaran, P.; Awasti, A.; Kim, H.; Mathew, B. Isatin-Tethered Halogen-Containing Acylhydrazone Derivatives as Monoamine Oxidase Inhibitor with Neuroprotective Effect. *Sci. Rep.* **2024**, *14*, 1264. [CrossRef]
16. Altıntop, M.D.; Ertorun, İ.; Akalın Çiftçi, G.; Özdemir, A. Design, Synthesis and Biological Evaluation of a New Series of Imidazothiazole-Hydrazone Hybrids as Dual EGFR and Akt Inhibitors for NSCLC Therapy. *Eur. J. Med. Chem.* **2024**, *276*, 116698. [CrossRef]
17. Tran, T.H.; Le, T.H.; Truong, H.N.; Dang, T.M.; Nguyen, M.T.T.; Nguyen, N.T.; Dang, P.H. Synthesis, Cytotoxicity, and Quantitative Structure–Activity Relationship Studies of Alkyl Triphenylphosphonium Pinostrobin Derivatives. *ChemistrySelect* **2024**, *9*, e202402190. [CrossRef]
18. Smirnova, A.; Tretyakova, E.; Kazakova, O. New Cytotoxic α-Aminoacylamide and *Bis* -1,5-Disubstituted Tetrazole Adducts From Amino-Diterpene Molecules by Ugi Reaction. *Chem. Biol. Drug Des.* **2024**, *104*, e14632. [CrossRef]
19. Çınarlı, M.; Ataol, Ç.Y.; Zeyrek, C.T.; Öğütcü, H.; Açık, L.; Batı, H. Design, Synthesis, Characterization, Theoretical Calculations, Molecular Docking Studies, and Biological Evaluation of New Fe(II) and Cu(II) Complexes of 2-Acetylpyridine Derivative Sulfonyl Hydrazone Schiff Base. *J. Mol. Struct.* **2025**, *1321*, 140112. [CrossRef]
20. Chen, F.; Jiang, Y.; Xu, Z.; Zhao, D.; Li, D.; Yang, H.; Zhu, S.; Xu, H.; Peng, S.; Miao, Z.; et al. Design, Synthesis and Evaluation of Novel LpxC Inhibitors Containing a Hydrazone Moiety as Gram-Negative Antibacterial Agents. *Eur. J. Med. Chem.* **2024**, *279*, 116892. [CrossRef]
21. Kamat, V.; Venuprasad, K.D.; Shadakshari, A.J.; Bhat, R.S.; D'souza, A.; Chapi, S.; Kumar, A.; Kuthe, P.V.; Sankaranarayanan, M.; Venugopala, K.N. Synthesis, Anti-Inflammatory, Antibacterial, and Antioxidant Evaluation of Novel Pyrazole-Linked Hydrazone Derivatives. *J. Mol. Struct.* **2024**, *1312*, 138634. [CrossRef]
22. Zang, Z.-L.; Wang, Y.-X.; Battini, N.; Gao, W.-W.; Zhou, C.-H. Synthesis and Antibacterial Medicinal Evaluation of Carbothioamido Hydrazonyl Thiazolylquinolone with Multitargeting Antimicrobial Potential to Combat Increasingly Global Resistance. *Eur. J. Med. Chem.* **2024**, *275*, 116626. [CrossRef] [PubMed]
23. Siutkina, A.I.; Chashchina, S.V.; Makhmudov, R.R.; Novikova, V.V.; Igidov, N.M.; Chernov, I.N. Synthesis, Analgesic and Antimicrobial Activity of N-Hetarylamides of 2-(2-(Diarylmethylene)Hydrazono)-5,5-Dimethyl-4-Oxohexanoic Acid. *Izv. Vyss. Uchebnykh Zaved. Khimiya Khimicheskaya Tekhnologiya* **2022**, *65*, 74–82. [CrossRef]
24. Althagafy, H.S.; El-Aziz, M.K.A.; Ibrahim, I.M.; Abd-alhameed, E.K.; Hassanein, E.H.M. Pharmacological Updates of Nifuroxazide: Promising Preclinical Effects and the Underlying Molecular Mechanisms. *Eur. J. Pharmacol.* **2023**, *951*, 175776. [CrossRef] [PubMed]
25. Kumbhar, P.; Kole, K.; Yadav, T.; Bhavar, A.; Waghmare, P.; Bhokare, R.; Manjappa, A.; Jha, N.K.; Chellappan, D.K.; Shinde, S.; et al. Drug Repurposing: An Emerging Strategy in Alleviating Skin Cancer. *Eur. J. Pharmacol.* **2022**, *926*, 175031. [CrossRef]
26. Sah, P.P.T.; Peoples, S.A. Isonicotinyl Hydrazones as Antitubercular Agents and Derivatives for Identification of Aldehydes and Ketones. *J. Am. Pharm. Assoc. (Sci. Ed.)* **1954**, *43*, 513–524. [CrossRef]
27. Palmer, L.D.; Skaar, E.P. Transition Metals and Virulence in Bacteria. *Annu. Rev. Genet.* **2016**, *50*, 67–91. [CrossRef]
28. Sada, P.K.; Bar, A.; Jassal, A.K.; Kumar, P.; Srikrishna, S.; Singh, A.K.; Kumar, S.; Singh, L.; Rai, A. A Novel Rhodamine Probe Acting as Chemosensor for Selective Recognition of Cu2+ and Hg2+ Ions: An Experimental and First Principle Studies. *J. Fluoresc.* **2024**, *34*, 2035–2055. [CrossRef]
29. Anitha, O.; Ghorai, S.; Thiruppathiraja, T.; Amir, H.; Murugan, A.; Natarajan, R.; Lakshmipathi, S.; Viswanathan, C.; Jothi, M.; Murugesapandian, B. Pyridine Appended Pyrimidine Bis Hydrazone: Zn2+/ATP Detection, Bioimaging and Functional Properties of Its Dinuclear Zn(II) Complex. *Talanta* **2024**, *273*, 125900. [CrossRef]

30. Musikavanhu, B.; Huang, Z.; Ma, Q.; Liang, Y.; Xue, Z.; Feng, L.; Zhao, L. A Pyridine Modified Naphthol Hydrazone Schiff Base Chemosensor for Al3+ via Intramolecular Charge Transfer Process. *Spectrochim. Acta Part A Mol. Biomol. Spectrosc.* **2023**, *301*, 122961. [CrossRef]
31. Wang, J.; Zhou, Y.; Si, G.; Xu, G.; Zhou, S.; Xue, X. A New Turn on Coumarin-Based Fluorescence Probe for Cr3+ Detection in Aqueous Solution. *J. Inorg. Biochem.* **2023**, *247*, 112302. [CrossRef]
32. Dewangan, S.; Mishra, A.; Halder, B.; Mishra, A.; Dhiman, R.; Chatterjee, S. Unsymmetrically Bi-Functionalized 1,1′-Ferrocenyl Bi-Hydrazone and Hydrazone-Cyanovinyl Molecules as Fluorescent "on–off" Sensor: Synthesis, Cytotoxicity and Cancer Cell Imaging Behavior. *Inorganica Chim. Acta* **2023**, *552*, 121511. [CrossRef]
33. Turhan, O.; Yaman, M.; Dikmen, G.; Nural, Y.; Sarıboyacı, A.E.; Tasa, B.A.; Soykan, M.N.; Seferoğlu, Z. Novel Fluorescent Sensors Based on Coumarin-Hydrazide-Hydrazone Hybrid for the Detection of CN−, Co2+ and Ni2+ Ions: DFT and Bioimaging in Living Cells. *J. Mol. Liq.* **2023**, *392*, 123440. [CrossRef]
34. Zhang, C.; Zhang, X.; Zhou, Z. Dual-Site Lysosome-Targeted Fluorescent Sensor for Fast Distinguishing Visualization of HClO and ONOO– in Living Cells and Zebrafish. *Spectrochim. Acta Part A Mol. Biomol. Spectrosc.* **2024**, *312*, 124064. [CrossRef] [PubMed]
35. Guo, F.-F.; Wang, B.-B.; Wu, W.-N.; Bi, W.-Y.; Xu, Z.-H.; Fan, Y.-C.; Bian, L.-Y.; Wang, Y. A Pyrazine-Containing Hydrazone Derivative for Sequential Detection of Al3+ and F−. *J. Mol. Struct.* **2022**, *1251*, 132073. [CrossRef]
36. Wang, L.; Wu, S.; Tang, H.; Meier, H.; Cao, D. An Efficient Probe for Sensing Different Concentration Ranges of Glutathione Based on AIE-Active Schiff Base Nanoaggregates with Distinct Reaction Mechanism. *Sens. Actuators B Chem.* **2018**, *273*, 1085–1090. [CrossRef]
37. Guo, X.; Gao, W.; Cheng, Z.-Z.; Huang, Y.-Y.; Yao, Z.-Y.; Li, Q.-Z.; Qiao, X.; Xie, C.-Z.; Xu, J.-Y. Highly Selective Fluorescent Detection Platform Based on Isoquinoline Schiff Base Ligand Monitors Glutathione in Biological Systems. *J. Photochem. Photobiol. A Chem.* **2022**, *428*, 113864. [CrossRef]
38. Zhou, H.; Huang, X.; Zheng, S.; Guo, H.; Yang, F. An Effect Fluorescence Sensor for Arginine Based on Bis-Cyanodistyrene Schiff-Base. *J. Mol. Struct.* **2024**, *1305*, 137798. [CrossRef]
39. Gnocchini, E.; Pilesi, E.; Schiano, L.; Vernì, F. Vitamin B6 Deficiency Promotes Loss of Heterozygosity (LOH) at the Drosophila Warts (Wts) Locus. *IJMS* **2022**, *23*, 6087. [CrossRef]
40. Barile, A.; Graziani, C.; Antonelli, L.; Parroni, A.; Fiorillo, A.; Di Salvo, M.L.; Ilari, A.; Giorgi, A.; Rosignoli, S.; Paiardini, A.; et al. Identification of the Pyridoxal 5′-phosphate Allosteric Site in Human Pyridox(Am)Ine 5′-phosphate Oxidase. *Protein Sci.* **2024**, *33*, e4900. [CrossRef]
41. Pilesi, E.; Angioli, C.; Graziani, C.; Parroni, A.; Contestabile, R.; Tramonti, A.; Vernì, F. A Gene-nutrient Interaction between Vitamin B6 and Serine Hydroxymethyltransferase (SHMT) Affects Genome Integrity in *Drosophila*. *J. Cell. Physiol.* **2023**, *238*, 1558–1566. [CrossRef]
42. Moosa, N.Y.; Azeem, S.A.; Lodge, J.K.; Cheung, W.; Ahmed, S.U. Vitamin B6 Pathway Maintains Glioblastoma Cell Survival in 3D Spheroid Cultures. *IJMS* **2024**, *25*, 10428. [CrossRef]
43. Graziani, C.; Barile, A.; Antonelli, L.; Fiorillo, A.; Ilari, A.; Vetica, F.; Di Salvo, M.L.; Paiardini, A.; Tramonti, A.; Contestabile, R. The *Z* Isomer of Pyridoxilidenerhodanine 5′-phosphate Is an Efficient Inhibitor of Human Pyridoxine 5′-phosphate Oxidase, a Crucial Enzyme in Vitamin B_6 Salvage Pathway and a Potential Chemotherapeutic Target. *FEBS J.* **2024**, *291*, 4984–5001. [CrossRef]
44. Gálvez-Navas, J.M.; Molina-Montes, E.; Rodríguez-Barranco, M.; Ramírez-Tortosa, M.; Gil, Á.; Sánchez, M.-J. Molecular Mechanisms Linking Genes and Vitamins of the Complex B Related to One-Carbon Metabolism in Breast Cancer: An In Silico Functional Database Study. *IJMS* **2024**, *25*, 8175. [CrossRef] [PubMed]
45. Pilesi, E.; Tesoriere, G.; Ferriero, A.; Mascolo, E.; Liguori, F.; Argirò, L.; Angioli, C.; Tramonti, A.; Contestabile, R.; Volontè, C.; et al. Vitamin B6 Deficiency Cooperates with Oncogenic Ras to Induce Malignant Tumors in Drosophila. *Cell Death Dis.* **2024**, *15*, 388. [CrossRef] [PubMed]
46. He, C.; Wang, D.; Shukla, S.K.; Hu, T.; Thakur, R.; Fu, X.; King, R.J.; Kollala, S.S.; Attri, K.S.; Murthy, D.; et al. Vitamin B6 Competition in the Tumor Microenvironment Hampers Antitumor Functions of NK Cells. *Cancer Discov.* **2024**, *14*, 176–193. [CrossRef] [PubMed]
47. Ponka, P.; Borova, J.; Neuwirt, J.; Fuchs, O. Mobilization of Iron from Reticulocytes: Identification of Pyridoxal Isonicotinoyl Hydrazone as a New Iron Chelating Agent. *FEBS Lett.* **1979**, *97*, 317–321. [CrossRef]
48. Ponka, P.; Richardson, D.R.; Edward, J.T.; Chubb, F.L. Iron Chelators of the Pyridoxal Isonicotinoyl Hydrazone Class. Relationship of the Lipophilicity of the Apochelator to Its Ability to Mobilise Iron from Reticulocytes in Vitro. *Can. J. Physiol. Pharmacol.* **1994**, *72*, 659–666. [CrossRef]
49. Hermes-Lima, M.; Nagy, E.; Ponka, P.; Schulman, H.M. The Iron Chelator Pyridoxal Isonicotinoyl Hydrazone (PIH) Protects Plasmid pUC-18 DNA against OH-Mediated Strand Breaks. *Free Radic. Biol. Med.* **1998**, *25*, 875–880. [CrossRef]
50. Szuber, N.; Buss, J.L.; Soe-Lin, S.; Felfly, H.; Trudel, M.; Ponka, P. Alternative Treatment Paradigm for Thalassemia Using Iron Chelators. *Exp. Hematol.* **2008**, *36*, 773–785. [CrossRef]

51. Richardson, D.R.; Milnes, K. The Potential of Iron Chelators of the Pyridoxal Isonicotinoyl Hydrazone Class as Effective Antiproliferative Agents II: The Mechanism of Action of Ligands Derived From Salicylaldehyde Benzoyl Hydrazone and 2-Hydroxy-1-Naphthylaldehyde Benzoyl Hydrazone. *Blood* **1997**, *89*, 3025–3038. [CrossRef]
52. Gao, J.; Richardson, D.R. The Potential of Iron Chelators of the Pyridoxal Isonicotinoyl Hydrazone Class as Effective Antiproliferative Agents, IV: The Mechanisms Involved in Inhibiting Cell-Cycle Progression. *Blood* **2001**, *98*, 842–850. [CrossRef]
53. Karwt, R.; Bondar, O.V.; Pugachev, M.V.; Mohammad, T.; Kadyrova, A.S.; Pavelyev, R.S.; Alrhmoun, S.; Gnezdilov, O.I.; Shtyrlin, Y.G. Anticancer Potential of Pyridoxine-Based Doxorubicin Derivatives: An In Vitro Study. *Life* **2024**, *14*, 282. [CrossRef] [PubMed]
54. Bhattacharya, M.; Ponka, P.; Hardy, P.; Hanna, N.; Varma, D.R.; Lachapelle, P.; Chemtob, S. Prevention of Postasphyxia Electroretinal Dysfunction with a Pyridoxal Hydrazone. *Free Radic. Biol. Med.* **1997**, *22*, 11–16. [CrossRef] [PubMed]
55. Ponka, P.; Schulman, H.M.; Wilczynska, A. Ferric Pyridoxal Isonicotinol Hydrazone Can Provide Iron for Heme Synthesis in Reticulocytes. *Biochim. Et Biophys. Acta (BBA)-Gen. Subj.* **1982**, *718*, 151–156. [CrossRef]
56. Huang, A.; Ponka, P. A Study of the Mechanism of Action of Pyridoxal Isonicotinoyl Hydrazone at the Cellular Level Using Reticulocytes Loaded with Non-Heme 59Fe. *Biochim. Et Biophys. Acta (BBA)-Gen. Subj.* **1983**, *757*, 306–315. [CrossRef]
57. Buss, J.L.; Neuzil, J.; Gellert, N.; Weber, C.; Ponka, P. Pyridoxal Isonicotinoyl Hydrazone Analogs Induce Apoptosis in Hematopoietic Cells Due to Their Iron-Chelating Properties. *Biochem. Pharmacol.* **2003**, *65*, 161–172. [CrossRef]
58. Buss, J.L.; Neuzil, J.; Ponka, P. The Role of Oxidative Stress in the Toxicity of Pyridoxal Isonicotinoyl Hydrazone (PIH) Analogues. *Biochem. Soc. Trans.* **2002**, *30*, 755–758. [CrossRef]
59. Casas, J.S.; Couce, M.D.; Sordo, J. Coordination Chemistry of Vitamin B6 and Derivatives: A Structural Overview. *Coord. Chem. Rev.* **2012**, *256*, 3036–3062. [CrossRef]
60. Sahoo, S.K. Chromo-Fluorogenic Sensing Using Vitamin B_6 Cofactors and Their Derivatives: A Review. *New J. Chem.* **2021**, *45*, 8874–8897. [CrossRef]
61. Richardson, D.R.; Wis Vitolo, L.M.; Hefter, G.T.; May, P.M.; Clare, B.W.; Webb, J.; Wilairat, P. Iron Chelators of the Pyridoxal Isonicotinoyl Hydrazone Class Part I. Ionisation Characteristics of the Ligands and Their Relevance to Biological Properties. *Inorganica Chim. Acta* **1990**, *170*, 165–170. [CrossRef]
62. Wis Vitolo, L.M.; Hefter, G.T.; Clare, B.W.; Webb, J. Iron Chelators of the Pyridoxal Isonicotinoyl Hydrazone Class Part II. Formation Constants with Iron(III) and Iron(II). *Inorganica Chim. Acta* **1990**, *170*, 171–176. [CrossRef]
63. Bertrand, B.; Williams, M.R.M.; Bochmann, M. Gold(III) Complexes for Antitumor Applications: An Overview. *Chem. A Eur. J* **2018**, *24*, 11840–11851. [CrossRef]
64. Gurba, A.; Taciak, P.; Sacharczuk, M.; Młynarczuk-Biały, I.; Bujalska-Zadrożny, M.; Fichna, J. Gold (III) Derivatives in Colon Cancer Treatment. *IJMS* **2022**, *23*, 724. [CrossRef] [PubMed]
65. Ratia, C.; Sueiro, S.; Soengas, R.G.; Iglesias, M.J.; López-Ortiz, F.; Soto, S.M. Gold(III) Complexes Activity against Multidrug-Resistant Bacteria of Veterinary Significance. *Antibiotics* **2022**, *11*, 1728. [CrossRef] [PubMed]
66. Kuranova, N.N.; Pimenov, O.A.; Zavalishin, M.N.; Gamov, G.A. Complexes of Gold(III) with Hydrazones Derived from Pyridoxal: Stability, Structure, and Nature of UV-Vis Spectra. *IJMS* **2024**, *25*, 5046. [CrossRef] [PubMed]
67. Patanjali, P.; Kumar, R.; Sourabh; Kumar, A.; Chaudhary, P.; Singh, R. Reviewing Gold(III) Complexes as Effective Biological Operators. *Main Group Chem.* **2018**, *17*, 35–52. [CrossRef]
68. Wróblewska, A.; Sadowski, M.; Jasiński, R. Selectivity and Molecular Mechanism of the Au(III)-Catalyzed [3+2] Cycloaddition Reaction between (Z)-C,N-Diphenylnitrone and Nitroethene in the Light of the Molecular Electron Density Theory Computational Study. *Chem Heterocycl Comp* **2024**, *60*, 639–645. [CrossRef]
69. Zavalishin, M.N.; Maltseva, M.A.; Osokin, V.S.; Aleksandriiskii, V.V.; Petrova, U.A.; Knyazeva, A.A.; Eroshin, A.V.; Zhabanov, Y.A.; Gamov, G.A. Synthesis and Characterization of a Vitamin B6-Tetrazole Hydrazone as a Fluorescence Probe for Selective Detection of Cd2+ and Ga3+ Ions. *Opt. Mater.* **2025**, *158*, 116493. [CrossRef]
70. Gamov, G.A.; Kiselev, A.N.; Aleksandriiskii, V.V.; Sharnin, V.A. Influence of Regioisomerism on Stability, Formation Kinetics and Ascorbate Oxidation Preventive Properties of Schiff Bases Derived from Pyridinecarboxylic Acids Hydrazides and Pyridoxal 5′-Phosphate. *J. Mol. Liq.* **2017**, *242*, 1148–1155. [CrossRef]
71. Gamov, G.A.; Khodov, I.A.; Belov, K.V.; Zavalishin, M.N.; Kiselev, A.N.; Usacheva, T.R.; Sharnin, V.A. Spatial Structure, Thermodynamics and Kinetics of Formation of Hydrazones Derived from Pyridoxal 5′-Phosphate and 2-Furoic, Thiophene-2-Carboxylic Hydrazides in Solution. *J. Mol. Liq.* **2019**, *283*, 825–833. [CrossRef]
72. Zavalishin, M.N.; Gamov, G.A.; Pogonin, A.E.; Isagulieva, A.K.; Shibaeva, A.V.; Klimovich, M.A.; Morozov, V.N. A New Fluorescent Vitamin B6-Based Probe for Selective and Sensitive Detection Ga3+ Ions in the Environment and Living Cells. *Dye. Pigment.* **2023**, *219*, 111621. [CrossRef]
73. Kuranova, N.N.; Petrova, D.V.; Zavalishin, M.N.; Kiselev, A.N.; Gamov, G.A. Prediction of Protonation Constants of Hydrazones and Schiff Bases Derived from Pyridoxal 5′-Phosphate, Pyridoxal, 3-Hydroxyisonicotinaldehyde and Salicylic Aldehyde. *J. Mol. Liq.* **2023**, *390*, 123049. [CrossRef]

74. Molinspiration Calculation of Molecular Properties and Bioactivity Score. Available online: https://www.molinspiration.com/cgi/properties (accessed on 17 October 2024).
75. Zavalishin, M.N.; Gamov, G.A.; Nikitin, G.A.; Pimenov, O.A.; Aleksandriiskii, V.V.; Isagulieva, A.K.; Shibaeva, A.V. A Simple Vitamin B6-Based Fluorescent Chemosensor for Selective and Sensitive Al3+ Recognition in Water: A Spectral and DFT Study. *Microchem. J.* **2024**, *197*, 109791. [CrossRef]
76. Patil, S.; Kuman, M.M.; Palvai, S.; Sengupta, P.; Basu, S. Impairing Powerhouse in Colon Cancer Cells by Hydrazide–Hydrazone-Based Small Molecule. *ACS Omega* **2018**, *3*, 1470–1481. [CrossRef]
77. Srovnalová, A.; Kaplánek, R.; Kejík, Z.; Hajduch, J.; Gurská, S.; Martásek, P.; Hajdúch, M.; Džubák, P.; Jakubek, M. Synthesis and Evaluation of Cyclobut-3-Ene-1,2-Dione-3-Hydrazones with Benzothiazole Moiety as Novel Anticancer Agents Inducing Nonapoptotic Oncosis-like Cell Death. *Biomed. Pharmacother.* **2025**, *190*, 118404. [CrossRef]
78. Negru, G.; Kamus, L.; Bîcu, E.; Shova, S.; Sendid, B.; Dubar, F.; Ghinet, A. Attempts to Access a Series of Pyrazoles Lead to New Hydrazones with Antifungal Potential against Candida Species Including Azole-Resistant Strains. *Molecules* **2021**, *26*, 5861. [CrossRef]
79. Başaran, E.; Tür, G.; Akkoc, S.; Taskin-Tok, T. Design, Synthesis, and In Silico and In Vitro Cytotoxic Activities of Novel Isoniazid–Hydrazone Analogues Linked to Fluorinated Sulfonate Esters. *ACS Omega* **2024**, *9*, 17551–17562. [CrossRef]
80. Liu, R.; Cui, J.; Ding, T.; Liu, Y.; Liang, H. Research Progress on the Biological Activities of Metal Complexes Bearing Polycyclic Aromatic Hydrazones. *Molecules* **2022**, *27*, 8393. [CrossRef]
81. Tafere, D.A.; Gebrezgiabher, M.; Elemo, F.; Sani, T.; Atisme, T.B.; Ashebr, T.G.; Ahmed, I.N. Hydrazones, Hydrazones-Based Coinage Metal Complexes, and Their Biological Applications. *RSC Adv.* **2025**, *15*, 6191–6207. [CrossRef]
82. Yeo, C.I.; Goh, C.H.P.; Tiekink, E.R.T.; Chew, J. Antibiotics: A "GOLDen" Promise? *Coord. Chem. Rev.* **2024**, *500*, 215429. [CrossRef]
83. Zavalishin, M.N.; Kiselev, A.N.; Pechnikova, N.L.; Shagalov, E.V.; Nikitin, G.A.; Gamov, G.A. Benzotiazole-Based Colorimetric Chemosensor for the Effective Detection of Hazardous Cyanide Ions. *ChemistrySelect* **2023**, *8*, e202301302. [CrossRef]
84. Gamov, G.A.; Zavalishin, M.N. La3+, Ce3+, Eu3+, and Gd3+ Complex Formation with Hydrazones Derived from Pyridoxal 5′-Phosphate in a Neutral Tris–HCl Buffer. *Russ. J. Inorg. Chem.* **2021**, *66*, 1561–1568. [CrossRef]
85. Khodov, I.A.; Belov, K.V.; Pogonin, A.E.; Savenkova, M.A.; Gamov, G.A. Spatial Structure and Conformations of Hydrazones Derived from Pyridoxal 5′-Phosphate and 2-, 3-Pyridinecarbohydrazide in the Light of NMR Study and Quantum Chemical Calculations. *J. Mol. Liq.* **2021**, *342*, 117372. [CrossRef]
86. Zavalishin, M.N.; Gamov, G.A.; Pimenov, O.A.; Pogonin, A.E.; Aleksandriiskii, V.V.; Usoltsev, S.D.; Marfin, Y.S. Pyridoxal 5′-Phosphate 2-Methyl-3-Furoylhydrazone as a Selective Sensor for Zn2+ Ions in Water and Drug Samples. *J. Photochem. Photobiol. A Chem.* **2022**, *432*, 114112. [CrossRef]
87. Liu, M.; Mao, X.; Ye, C.; Huang, H.; Nicholson, J.K.; Lindon, J.C. Improved WATERGATE Pulse Sequences for Solvent Suppression in NMR Spectroscopy. *J. Magn. Reson.* **1998**, *132*, 125–129. [CrossRef]

Disclaimer/Publisher's Note: The statements, opinions and data contained in all publications are solely those of the individual author(s) and contributor(s) and not of MDPI and/or the editor(s). MDPI and/or the editor(s) disclaim responsibility for any injury to people or property resulting from any ideas, methods, instructions or products referred to in the content.